AAAS
Ultrafast Science
Volume 2022, Article ID 9863548, 9 pages
https://doi.org/10.34133/2022/9863548

Ultrafast Science
A SCIENCE PARTNER JOURNAL

Research Article

Low-Energy Protons in Strong-Field Dissociation of H_2^+ via Dipole-Transitions at Large Bond Lengths

Shengzhe Pan,[1] Chenxi Hu,[2] Zhaohan Zhang,[2] Peifen Lu,[1] Chenxu Lu,[1] Lianrong Zhou,[1] Jiawei Wang,[1] Fenghao Sun,[1] Junjie Qiang,[1] Hui Li,[1] Hongcheng Ni,[1] Xiaochun Gong,[1] Feng He,[2,3] and Jian Wu[1,3,4]

[1]*State Key Laboratory of Precision Spectroscopy, East China Normal University, Shanghai 200241, China*
[2]*Key Laboratory for Laser Plasmas (Ministry of Education) and School of Physics and Astronomy, Collaborative Innovation Center of IFSA (CICIFSA), Shanghai Jiao Tong University, Shanghai 200240, China*
[3]*CAS Center for Excellence in Ultra-Intense Laser Science, Shanghai 201800, China*
[4]*Collaborative Innovation Center of Extreme Optics, Shanxi University, Taiyuan, Shanxi 030006, China*

Correspondence should be addressed to Feng He; fhe@sjtu.edu.cn and Jian Wu; jwu@phy.ecnu.edu.cn

Received 4 December 2021; Accepted 1 April 2022; Published 5 May 2022

More than ten years ago, the observation of the low-energy structure in the photoelectron energy spectrum, regarded as an "ionization surprise," has overthrown our understanding of strong-field physics. However, the similar low-energy nuclear fragment generation from dissociating molecules upon the photon energy absorption, one of the well-observed phenomena in light-molecule interaction, still lacks an unambiguous mechanism and remains mysterious. Here, we introduce a time-energy-resolved manner using a multicycle near-infrared femtosecond laser pulse to identify the physical origin of the light-induced ultrafast dynamics of molecules. By simultaneously measuring the bond-stretching times and photon numbers involved in the dissociation of H_2^+ driven by a polarization-skewed laser pulse, we reveal that the low-energy protons (below 0.7 eV) are produced via dipole-transitions at large bond lengths. The observed low-energy protons originate from strong-field dissociation of high vibrational states rather than the low ones of H_2^+ cation, which is distinct from the well-accepted bond-softening picture. Further numerical simulation of the time-dependent Schrödinger equation unveils that the electronic states are periodically distorted by the strong laser field, and the energy gap between the field-dressed transient electronic states may favor the one- or three-photon transitions at the internuclear distance larger than 5 a.u. The time-dependent scenario and our time-energy-resolved approach presented here can be extended to other molecules to understand the complex ultrafast dynamics.

1. Introduction

In ultrafast physics, the energy spectrum of electrons or nuclei is overwhelmingly crucial since it is the knob to retrieve atomic or molecular ultrafast dynamics. For example, the low-energy structure in the photoelectron energy spectrum [1, 2], regarded as an "ionization surprise" [3], has been used to unveil the importance of the field-driven rescattering in the long-range Coulomb potential [2, 4–10]. For molecules in intense laser fields, different dissociation pathways contribute to different nuclear fragment energies. For instance, the two-hump energy structure peaked around 0.7 and 1.2 eV of the ejected protons in the dissociation of H_2^+ driven by 790 nm lasers discloses the one-photon and net-two-photon pathways [11–15]. The vibrational states from which the dissociation starts are further identified by carefully analyzing the fine structure of the discrete energy peaks in the kinetic energy spectrum of the nuclear fragments [16, 17]. The production of the high-energy protons leads to the investigation of the above-threshold dissociation of H_2^+ [18, 19] and further the correlated electron-nuclear dynamics [20]. Here, we study the emission of low-energy protons in the dissociation of H_2^+, based on which an intriguing dissociation pathway is explored.

In the bond-softening scenario of molecular dissociation, it was believed that the low-energy fragments were contributed by the low vibrational states [21, 22]. For example, for a 790 nm driving laser pulse, H_2^+ in the $1s\sigma_g$ state absorbs

one photon resonantly at the internuclear distance of $R = 4.7$ a.u., and finally, the ejected proton has the energy spectrum peaked at 0.7 eV. For a stronger laser pulse, H_2^+ with even lower vibrational states may be excited, resulting in lower-energy fragments. While energy spectra of nuclear fragments boost our understanding of molecular dissociation, the lack of time information makes it hard to grasp the causality of chemical reactions. To thoroughly identify the physical origin, we need to clock the dissociation dynamics, particularly interests lying in a popularly employed multicycle laser pulse, in addition to the nuclear energy spectrum integrated over time.

In this article, we explore the low-energy protons in strong-field dissociative ionization of H_2 in a time-energy-resolved manner. The H_2 molecule is first singly ionized by the leading edge of a multicycle polarization-skewed (PS) laser pulse, producing H_2^+ to be dissociated by the remaining field of the same laser pulse. Our results reveal that the low-energy protons originate from the dissociation of the high vibrational states rather than the low ones of H_2^+, contrary to previous recognitions of the dissociation process [17, 22]. Bond-stretching times and photon numbers involved in the dissociation are extracted from the measured photoelectron angular distribution in the molecular frame. The time-dependent Schrödinger equation (TDSE) simulation for the dissociation of H_2^+ discovers one- or multiphoton dipole-transitions at large bond lengths, supporting the experimental observation and explanation.

2. Materials and Methods

2.1. Experimental Technique. We performed the experiment in an ultrahigh vacuum chamber of a cold target recoil ion momentum spectrometer [23, 24], where the photoelectrons and protons produced from the strong-field dissociative ionization of H_2 were detected in coincidence by two time- and position-sensitive microchannel plate detectors at the opposite ends of the spectrometer, as schematically illustrated in Figure 1. By measuring the time-of-flight and positions of the charged particle impacts, the three-dimensional momenta and kinetic energies of the photoelectrons and protons were reconstructed event-by-event during the offline analysis. The PS laser pulse is constructed by propagating a linearly polarized femtosecond laser pulse (28 fs, 790 nm) through a multiorder wave plate (MOWP) in conjunction with a Berek compensator (BC) (see [13, 15, 25] for more experimental details). The PS laser pulse propagates along the x axis, and its polarization rotates slowly from 135° (315°) to 45° (225°) in the y-z plane, shown as the red waveform in the inset of Figure 1. It is important to mention that the polarization of the PS laser pulse illustrated in Figure 1 is in the laboratory frame. The unique mapping between the cycle-changing polarization direction and its evolution time encodes the physical quantities into the molecular frame photoelectron angular distributions (MF-PADs).

2.2. Classical Model. In the classical model, the single ionization of H_2 in the PS laser pulse is described by $P_i(t)$ using the Ammosov-Delone-Krainov theory [26]. Then, the bond-stretching time τ of H_2^+ is calculated by solving the Newtonian equation $\mu d^2R/dt^2 = -dV(R)/dR$ [27] of a classical particle with reduced mass $\mu = 0.5m_{H^+}$, representing the nuclear wave packet (NWP) propagating on a certain potential energy curve $V(R)$ of H_2^+ [12–15], where R denotes the internuclear distance. Different initial kinetic energies are assigned for the classical particles to take into account the population of different vibrational states of the photoionization-launched NWPs. The dipole-transition rate $P_{nd}(t, \phi_{\mathrm{mol}}) \propto E^{2n}(t)\cos^{2n}[\phi_E(t) - \phi_{\mathrm{mol}}]$ is used to describe the n-photon resonant dipole-transition between the $1s\sigma_g$ and $2p\sigma_u$ states during the stretching of H_2^+ [28–30], where ϕ_E denotes the electric field direction of the laser pulse and ϕ_{mol} denotes the orientation of the molecular axis of H_2 in the laboratory frame. The whole probability of dissociative ionization can then be expressed by $P_{id}(t_i, \phi_{\mathrm{mol}}) = P_i(t_i)P_{nd}(t_i + \tau, \phi_{\mathrm{mol}})$, where t_i is the ionization instant of H_2. The emission direction of photoelectrons (ϕ_{ele}) is a function of t_i thanks to the fact that the motion of the photoelectron released at t_i is steered by the remaining laser field. By mapping the ionization instant to the photoelectron emission direction geared by the spatiotemporal profile of the PS pulse, we can transform the whole probability of dissociative ionization from $P_{id}(t_i, \phi_{\mathrm{mol}})$ into $P_{id}(\phi_{\mathrm{ele}}, \phi_{\mathrm{mol}})$. Here, the emission direction of protons (ϕ_{ion}) is the same as the molecular orientation (ϕ_{mol}), i.e., $\phi_{\mathrm{ion}} = \phi_{\mathrm{mol}}$, since the rotation of the molecular axis is negligible within the ultrafast dissociation process on the femtosecond timescale. Finally, after transforming from the laboratory frame, we achieve the photoelectron angular distribution in the molecular frame $P_{id}(\phi_{\mathrm{MF-ele}}) = P_{id}(\phi_{\mathrm{ele}} - \phi_{\mathrm{ion}})$.

2.3. Quantum Model. In the quantum model, we start from H_2^+ cation, which means the single ionization of H_2 is not included in the model. The dissociation process of H_2^+ is simulated numerically by solving the two-level TDSE under the Born-Oppenheimer approximation:

$$i\frac{\partial}{\partial t}\begin{pmatrix}\chi_g(R,t)\\ \chi_u(R,t)\end{pmatrix} = \begin{pmatrix}\hat{T} + V_g(R) & d_{gu}(R)E(t)\\ d_{gu}(R)E(t) & \hat{T} + V_u(R)\end{pmatrix}\begin{pmatrix}\chi_g(R,t)\\ \chi_u(R,t)\end{pmatrix}. \tag{1}$$

Here χ_g and χ_u are NWPs associated with the electron in the $1s\sigma_g$ and $2p\sigma_u$ states, respectively. V_g and V_u are the field-free potential energy curves for H_2^+ in the $1s\sigma_g$ and $2p\sigma_u$ states, respectively. $\hat{T}$ is the nuclear kinetic energy operator, $d_{gu}(R)$ is the R-dependent dipole between two electronic states, and E is the electric field of the incident laser pulse. The time and spatial steps are $dt = 0.1$ a.u. and $dR = 0.02$ a.u., respectively. R spans the range [0, 100] a.u. and is sampled by 5000 grids. The simulation area is large enough to hold all dissociating NWPs. We first use an imaginary-time propagation algorithm [31] to generate different vibrational states. Then, the Crank-Nicolson method [32] is adopted to propagate the NWP. Since we focus on

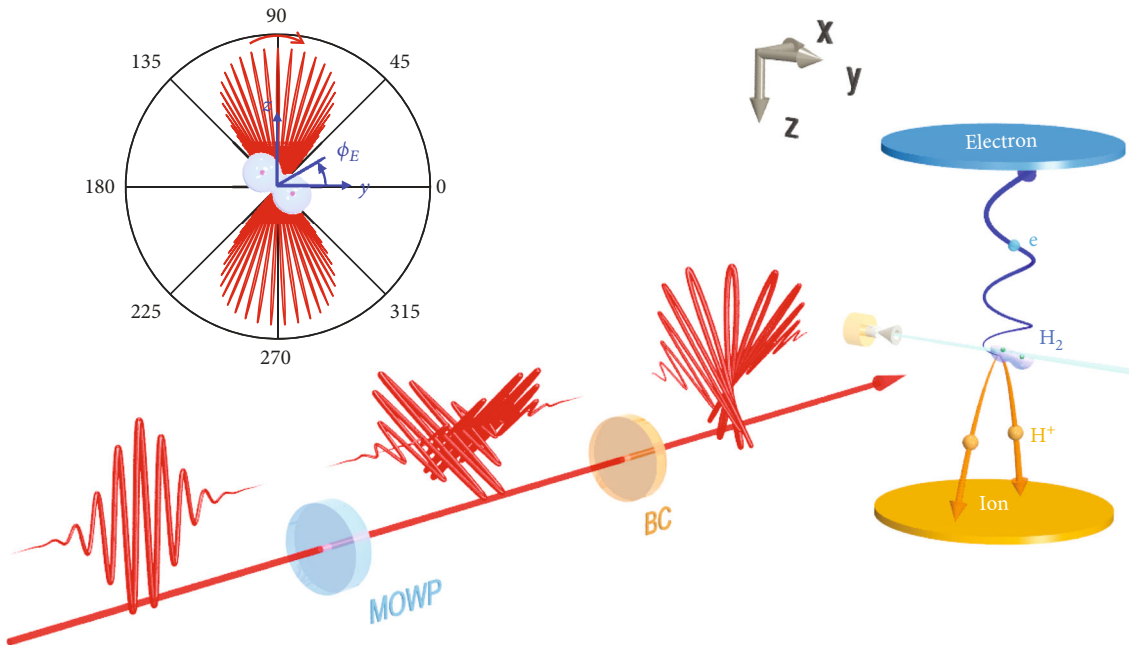

FIGURE 1: Schematic diagram of the experimental setup. The input femtosecond laser pulse (polarized along 90° in the y-z plane) is converted into two orthogonally polarized subpulses after the MOWP, whose relative phase is finely controlled by rotating the BC to construct the laser field with a desired spatiotemporal profile. The PS laser pulse with a rotating laser field is illustrated in the inset. Here the time delay between two orthogonally polarized components is $8T$, where $T = 2.6$ fs is the optical cycle of the input pulse. The peak intensity of the PS laser pulse in the interaction region was estimated to be $I_0 = 1 \times 10^{14}$ W/cm^2 by assuming the focusing volume of the PS pulse is the same as an incident linearly polarized reference pulse [36] and considering the orientation of the optical axis and orders of phase delay introduced by the wave plates in the beamline.

the dissociation dynamics for a given vibrational state, a linearly polarized laser pulse is better to unveil the mechanism. The laser pulse is written as $E(t) = E_0 \sin^2(\pi t/\tau_0) \cos(\omega t)$, where E_0 is the electric field amplitude, ω is the laser frequency, and τ_0 is the duration of the laser pulse. In the numerical simulation, the laser wavelength is 800 nm ($\omega = 0.057$ a.u.), and the laser pulse has the duration of ten optical cycles ($\tau_0 = 26.6$ fs). We assume that the initial vibrational state of H_2^+ is launched after the tunneling ionization of H_2 around the peak of the laser pulse. The dissociation process in the remaining field is simulated with the starting time $t = 600$ a.u., and a rising edge of a half cycle is adopted to avoid high-frequency components of the remaining field [33]. After the interaction with the laser pulse, the NWPs further propagate 2000 a.u. until the dissociation parts clearly separate from the bound parts.

3. Results and Discussion

As the orange arrow illustrated in Figure 2, H_2 is singly ionized at the equilibrium internuclear distance of R_e (~1.4 a.u.) when exposed to an intense laser field [11, 12]. The produced H_2^+ stretches and further absorbs photons from the remaining laser field and dissociates via the well-known one-photon and net-two-photon pathways [11–15], shown as the red and blue arrows between black curves in Figure 2. For example, in the one-photon pathway, the stretching H_2^+ absorbs one photon at R_ω, transits to the $2p\sigma_u$ state, and dissociates along the $2p\sigma_u$ curve. For the net-two-photon pathway, the stretching H_2^+ absorbs three photons at $R_{3\omega}$ and transits to the $2p\sigma_u$ state. As it propagates on the $2p\sigma_u$ curve, the H_2^+ will emit one photon at R_ω and then transit back to the $1s\sigma_g$ state, ending the dissociation along the $1s\sigma_g$ curve. The aforementioned two pathways can be identified by diagnosing the KER spectrum. Usually, the protons with KER peaked around 0.7 and 1.2 eV are distinguished as the one-photon and net-two-photon pathways driven by 790 nm lasers, shown in the inset of Figure 2. While the energy spectra of nuclear fragments offer abundant information related to molecular dynamics on the one hand, on the other hand, the time information about ultrafast molecular changes is hard to be grasped. To fully understand the dissociation process, simultaneous time- and energy-resolved measurements are required.

The PS laser field works as a timer by mapping the instants to the emission directions of photoelectrons and nuclear fragments, which allows us to understand different dissociation pathways in time and energy fashion. Figures 3(b)–3(d) present the measured photoelectron momentum distributions in the molecular frame by gating the nuclear KER spectrum in different energy regions indicated in the inset of Figure 2. The corresponding MF-PADs are illustrated in Figure 4(a). Since the photoelectron emission direction maps the vector potential of the laser field at the ionization instant, the MF-PAD peaked at the deflection angle α with respect to the molecular orientation along

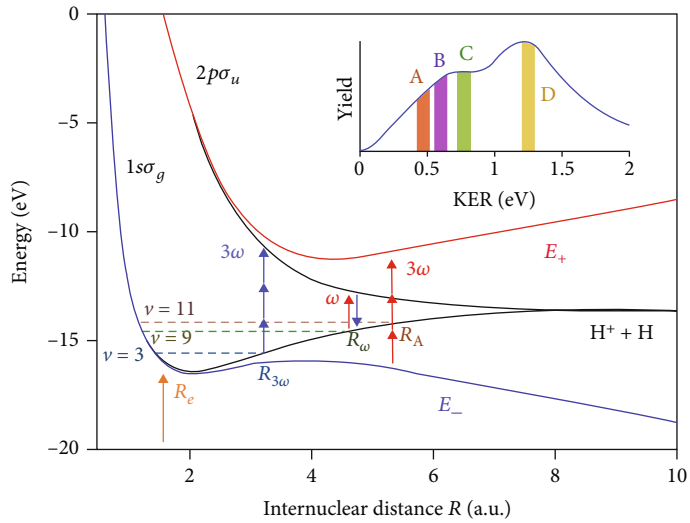

FIGURE 2: The potential energy curves of H_2^+. The orange arrow denotes the internuclear distance where ionization happens. The black curves illustrate the field-free $1s\sigma_g$ and $2p\sigma_u$ potential energy curves of H_2^+. The red and blue arrows between two black curves denote the one-photon and net-two-photon dissociation pathways, respectively. The red and blue curves are calculated using Equation (2) with a static electric field $E_0 = 0.038$ a.u. (corresponding to the intensity $I_0 = 5 \times 10^{13}$ W/cm^2). The red arrows between the red and blue curves denote the three-photon transitions between the two field-dressed transient electronic states. The dashed horizontal lines indicate the energies of vibrational states $v = 3$, $v = 9$, and $v = 11$ on the $1s\sigma_g$ potential energy curve. The inset (blue curve) shows the measured KER spectrum of the protons, where the highlighted four areas correspond to different dissociation pathways, respectively.

the y axis, as shown in Figure 3(a), records the bond-stretching time between the ionization instant of H_2 and the photon-coupled dipole-transition instant between the $1s\sigma_g$ and $2p\sigma_u$ states of H_2^+ during its dissociation. Physically, the dipole-transition rate of the stretching H_2^+ depends on the crossing angle between the molecular axis (ϕ_{mol}) and the laser polarization direction (ϕ_E) at transition instant, i.e., proportional to the $\cos^{2n}(\phi_E - \phi_{mol})$, where n is the number of the involved photons [28–30]. Since the single ionization of H_2 is entangled with the dissociation of H_2^+, the angular distribution of dissociative protons is encoded in the MF-PAD. In other words, the half width β of the MF-PAD illustrated in Figure 3(a) encodes the involved photon number n in the dissociation of H_2^+. Therefore, by extracting α and β of the MF-PAD, we can explore the light-induced stretching of the molecular ion in a time-energy fashion.

Figure 4(c) illustrates the normalized two-dimensional map of the MF-PADs versus nuclear KERs in experiments. The corresponding deflection angle α and half width β of the MF-PADs are extracted and plotted in Figure 4(d). The distinct distributions of α and β for KERs less or larger than 0.8 eV clearly confirm the previous assignment of the one-photon and net-two-photon dissociation pathways. The overall deflection angle α of high-energy range (KER~1.2 eV) is smaller than the one of low-energy range (KER~0.7 eV), denoting that the effective bond-stretching time (the photon-averaged time delay of the three-photon absorption and one-photon emission in the dissociation of H_2^+) of the net-two-photon pathway is shorter than the stretching time of one-photon pathway, which agrees with former observations [13] but the detailed KER-dependence is visualized here. The small value of β of the high-energy range implies that more photons are involved (including absorbed and emitted) in the net-two-photon pathway with respect to the one-photon pathway, which is surely within the expectation [13]. Surprisingly, for the low-energy fragments (KER < 0.7 eV), which have been believed to be originated from the low vibrational states of H_2^+ [17, 22], we observe an increasing deflection angle α and a decreasing half width β, i.e., a longer stretching time and more involved photons, as the decreasing of the KER to low values. In the following, we will unveil this new finding.

To get intuitive insights into the dissociation dynamics for the low-energy events, we calculate the MF-PADs using an intuitive classical model. In classical calculations, by assigning the initial kinetic energy of the NWP to match the energy of $v = 9$ vibrational state, i.e., $E_{k,0} = E_v - V_g(R_e)$, the bond-stretching time 11.8 fs of KER region C (one-photon pathway) is calculated by running the Newtonian equation on the $1s\sigma_g$ potential energy curve from R_e to R_ω, while the bond-stretching time 12.6 fs of KER region D (net-two-photon pathway) is calculated in the same way from R_e to $R_{3\omega}$ on the $1s\sigma_g$ curve and from $R_{3\omega}$ to R_ω on the $2p\sigma_u$ curve with the initial kinetic energy matching the energy of $v = 3$ vibrational state. Then, the quantitatively reproduced MF-PADs can be obtained if n is set to be 1 and 4 for KER regions of C and D, as shown by green and yellow curves in Figure 4(b). This conclusion is consistent with the well-accepted picture of the one-photon and net-two-photon dissociation pathways [11–15]. Here the KER region D, i.e., the net-two-photon pathway, is utilized to confirm the analysis process, and we will focus on the comparison between KER regions A, B, and C. To match the orange and violet

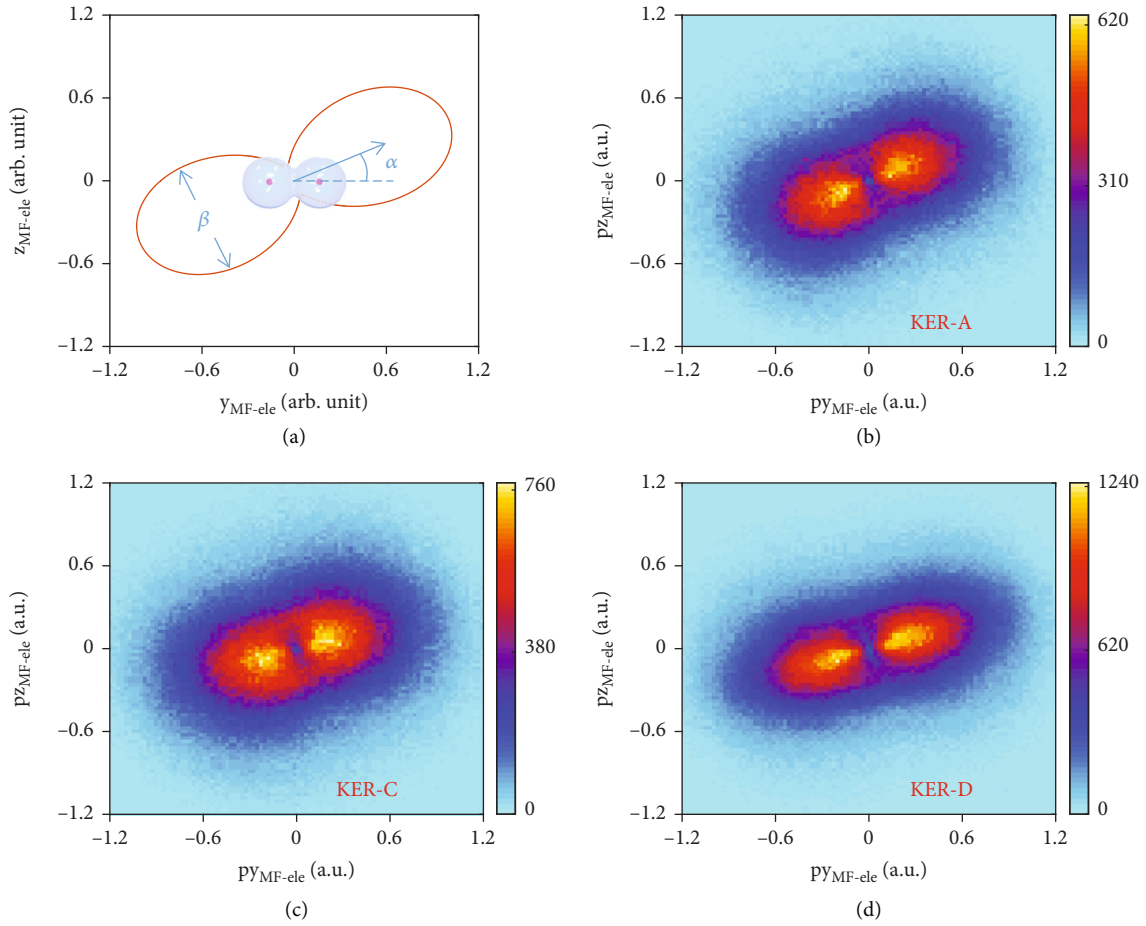

FIGURE 3: The photoelectron momentum distribution in the molecular frame. (a) The sketch of the photoelectron angular distribution (orange curve) in the molecular frame with the molecular orientation along the y axis. (b, d) Measured molecular frame electron momentum distributions corresponding to different regions in the nuclear KER spectrum highlighted in the inset of Figure 2.

curves in Figure 4(a), indicating the longer stretching time and more involved photons, one has to start from higher vibrational states. In the calculation, the initial kinetic energies of the NWPs for KER regions A and B are assigned to match the energies of $v = 11$ and 10 vibrational states, respectively. The transition bond lengths are also assigned to be the maximum internuclear distances of the corresponding vibrational states. With that, the good agreement of the MF-PADs between the experiments and calculations is achieved by setting $n = 1.2$ and 1.1. According to the classical simulation, the bond-stretching times of KER regions A and B are about 14.0 and 12.8 fs, respectively. Such long bond-stretching times observed here undoubtedly illustrate that there is a novel dissociation pathway giving rise to low-energy protons beyond traditional bond-softening scenarios.

We note that the energy gap between two field-free potential energy curves of the $1s\sigma_g$ and $2p\sigma_u$ states at the internuclear distance of R_A is much smaller than the photon energy, implying barely traditional resonant dipole-transitions between field-free electronic states. To illustrate the physical origin of the dynamics of low-energy protons, and we adopt the adiabatic representation [34], where the field-dressed transient electronic states are as follows:

$$E_{\pm}(R,t) = \frac{V_g(R) + V_u(R)}{2} \pm \sqrt{\frac{\left[V_u(R) - V_g(R)\right]^2}{4} + \left[d_{gu}(R)E(t)\right]^2}. \tag{2}$$

Hence, photon-coupled transitions can still happen at R_A between the field-dressed electronic states, depicted with red and blue curves in Figure 2. The blue and red curves are calculated using Equation (2) with a static electric field of $E_0 = 0.038$ a.u. (corresponding to the intensity of $I_0 = 5 \times 10^{13}$ W/cm^2). With time evolution, the energy gap between the field-dressed electronic states periodically changes. When the energy gap approaches the photon energy, H_2^+ may absorb one photon and transit to the upper state. Furthermore, with increasing laser intensity, the energy gap between two field-dressed states becomes larger according to Equation (2) so that the three-photon transition can also happen between the two states. One-photon and three-photon resonant transitions may happen between the two field-dressed states at different internuclear distances or different instants. These photon-coupled transitions may finally contribute the same KER and thus inevitably interfere with each other, giving the expected photon number n between 1 and 3.

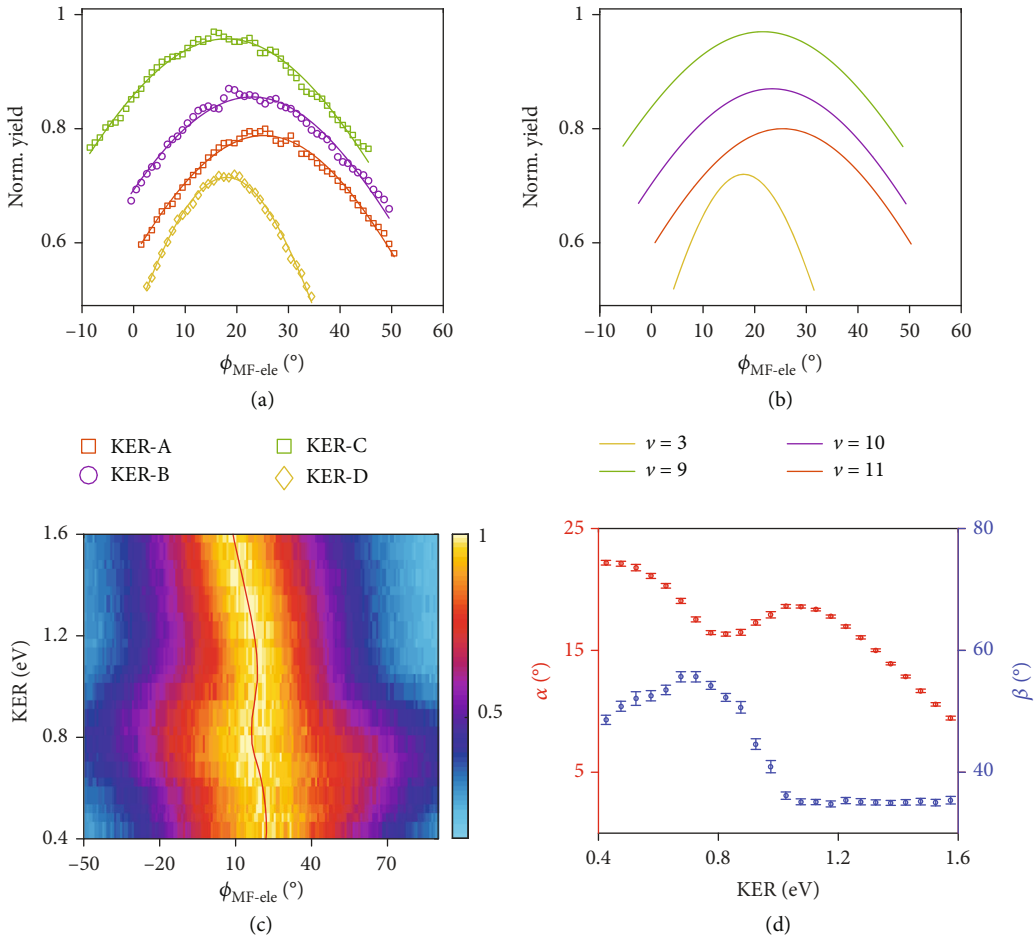

FIGURE 4: The molecular frame photoelectron angular distributions. (a) Measured MF-PADs are plotted for KER regions A (orange), B (violet), C (green), and D (yellow). (b) Classically simulated MF-PADs for dissociation pathway starting from $v = 3$ (yellow), $v = 9$ (green), $v = 10$ (violet), and $v = 11$ (orange). (c) Measured KER-dependent MF-PADS. The MF-PAD for each KER region is normalized to increase visibility. (d) Extracted deflection angle α and half width β of the MF-PADs.

To confirm the aforementioned intuitive scenario of the strong-field dissociation, we numerically solve Equation (1) to simulate the dissociation dynamics of a single vibrational state. Here, the initial vibrational state is $v = 11$ for the convenient analysis though other vibrational states give similar outputs. Figures 5(a) and 5(b) show the time evolutions of the density distributions and populations of χ_u driven by laser pulses with peak intensities $I_0 = 1 \times 10^{12}$ and 1×10^{14} W/cm^2, respectively, corresponding to the weak- and strong-field excitation regions. The corresponding normalized KER spectra are shown in Figure 5(c). We have to note that it is hard to define a specific internuclear distance in the pure quantum simulation since the up-down coupling between the ground and excited states occurs all the way with different probabilities and frequencies. Hence, the transition internuclear distances can only be obtained from the KER of the eventual outgoing NWP with the assistance of the classical scenario of the propagation on the potential energy curves. Considering the vibrational energy of the NWP centered around the $v = 11$ vibrational state, the mapping function of the internuclear distance to the KER of the dissociative fragments can be approximately described as $\text{KER} = E_v - V_g(R) + V_u(R) - V_u(+\infty)$, where E_v and $V_u(+\infty)$ denotes the energy of $v = 11$ vibrational state and the dissociation limit of the $2p\sigma_u$ state, respectively. According to the mapping function illustrated in Figure 5(d), the calculated KER spectrum peaks at around 1.2 eV in the weak-field case, indicating a resonant dipole-transition between $1s\sigma_g$ and $2p\sigma_u$ states at $R = 4.8$ a.u., as shown in Figure 5(e) (blue curve). The retrieved peak position is almost the same as the transition internuclear distance of the NWP centered around $v = 9$ vibrational state ($\sim R_\omega$), implying that the gain of the KER is mainly attributed to the more vibrational energy of the NWP centered around $v = 11$ vibrational state at R_ω. However, the KER has a very different distribution when using a strong laser field, as shown by the red curves in Figure 5(c). The shifted KER peak around 0.4 eV, corresponding to the KER region A in experiments, implies the dipole-transition mainly happens at $R = 5.6$ a.u. ($\sim R_A$) (red curve in Figure 5(e)). Though the energy gap between the field-free $1s\sigma_g$ and $2p\sigma_u$ states around R_A is far from the one- or three-photon energies, the field-dressed transient electronic states are favorable for the resonant transition at such a large internuclear distance.

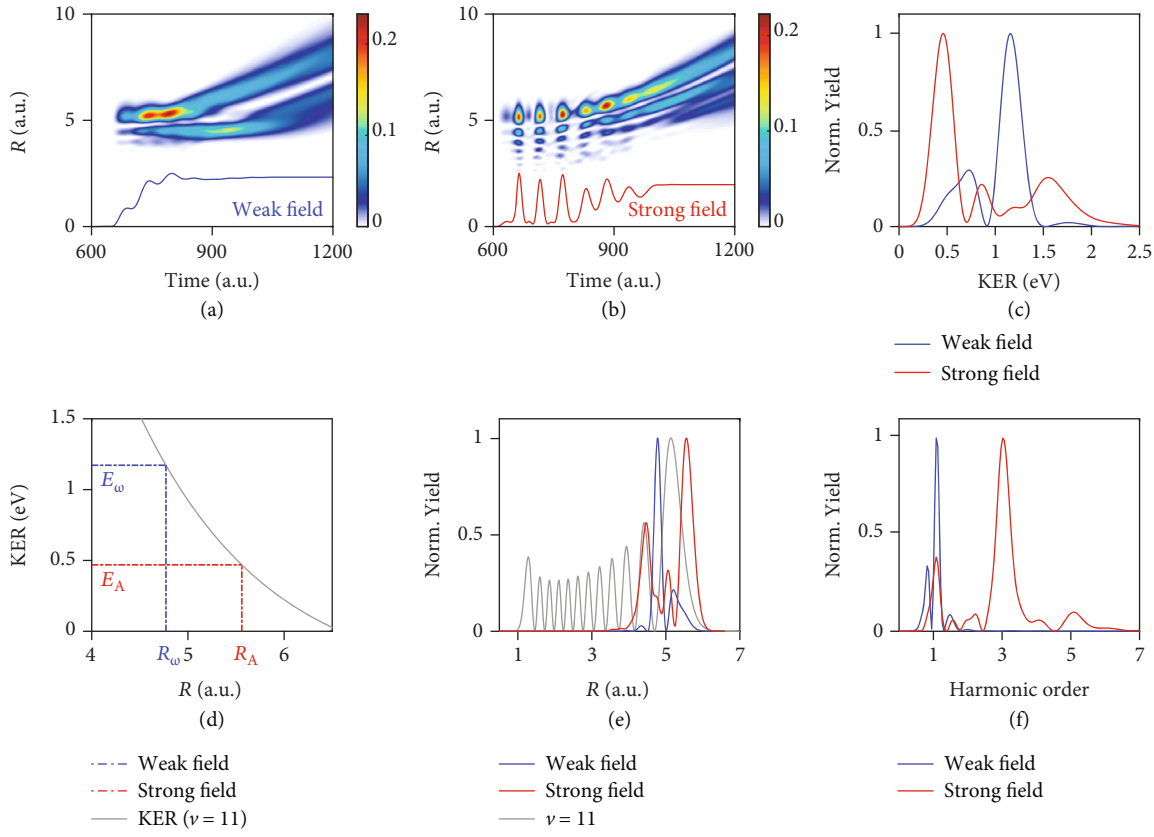

FIGURE 5: The TDSE simulation results. (a, b) Time evolutions of the density distribution of χ_u driven by laser pulses with the peak intensities (a) $I_0 = 1 \times 10^{12}$ W/cm^2 (weak field) and (b) $I_0 = 1 \times 10^{14}$ W/cm^2 (strong field). Corresponding populations of χ_u as a function of time are attached in the inset with arbitrary units. (c) KER spectra obtained from the dissociation of H_2^+ for the weak- and strong-field cases. (d) The mapping function of the internuclear distance to the KER of the dissociative fragments initialized from the $v = 11$ vibrational state. The blue and red dot-dashed lines denote the corresponding peak positions for the weak- and strong-field cases. (e) Retrieved distributions of the dissociating NWP from the eventually observed KER spectra for the weak- and strong-field cases. The initial distribution of the vibrational wave function of $v = 11$ is plotted as the gray curve. (f) Harmonic generation spectra of the dipole-transition obtained from the dissociation process driven by different peak intensities.

To further explore and verify that multiphoton transitions at large bond lengths have enrolled in the dissociation, we calculate the harmonic spectra by Fourier transforming the dipole acceleration. In the model, the dipole can be expressed as $d(t) = 2\,\mathrm{Re}\,[<\chi_g|d_{gu}(R)|\chi_u>]$. Figures 5(e) denotes the normalized harmonic generation with peak intensities $I_0 = 1 \times 10^{12}$ and 1×10^{14} W/cm^2, respectively. In the weak-field case, only the first harmonic order, corresponding to the single-photon transition, is observed, while in the strong-field case, the harmonic spectrum covers the first, third, and fifth orders, which indicates the coexistence of the one- and multiphoton transitions. The distribution of the harmonic spectrum can be manipulated by varying the laser intensity. For lower intensities, the lower orders have larger proportions. The harmonic spectrum enables us to directly verify the photon-coupled transitions between two field-dressed electronic states of H_2^+ [35]. Please note that the aforementioned strong-field dissociation process dominates only for a high vibrational state. For the NWP centered at $v = 9$ vibrational state, the dipole-transition mostly happens at a small internuclear distance ($\sim R_\omega$), rather than the large internuclear distances, for the NWP hardly distributes at large internuclear distances. The result also verifies the previous experimental results that the KER of the dissociation from the $v = 9$ vibrational state is hardly affected by the peak intensity of the near-infrared laser pulse [22].

4. Conclusion

In conclusion, energy-resolved measurements of the nuclear fragments are far from enough to comprehensively figure out the response of molecules in strong laser fields. Our time-energy-resolved proton-electron coincidence measurements using the PS laser field reveal that the low-energy structure in the nuclear KER spectrum originates from the dissociation of high vibrational states via absorbing one or multiple photons at internuclear distances far-beyond resonant transition between field-free potential energy curves. This picture is distinct from the well-accepted bond-softening scenario, in particular the production of the low-energy protons in strong-field dissociative ionization of H_2. The approach presented here can be extended to other molecules to understand the complex ultrafast strong-field dynamics.

Data Availability

The data that support the findings of this study are available from the corresponding author upon reasonable request.

Conflicts of Interest

The authors declare that there is no conflict of interest regarding the publication of this article.

Authors' Contributions

S. Pan and J. Wu conceived and designed the experiments; S. Pan, P. Lu, C. Lu, L. Zhou, J. Wang, F. Sun, J. Qiang, H. Li, X. Gong, and J. Wu performed the measurements and data analysis; S. Pan, C. Hu, Z. Zhang, H. Ni, and F. He developed the theoretical model and carried out the calculations. All authors discussed the results and contributed to the writing of the manuscript.

Acknowledgments

This work was supported by the National Key R&D Program of China (Grant Nos. 2018YFA0306303 and 2018YFA0404802), the National Natural Science Fund (Grant Nos. 11834004, 11621404, 11925405, and 91850203), the 111 Project of China (Grant No. B12024), Projects from Shanghai Science and Technology Commission (Grant No. 19JC1412200), and the Innovation Program of Shanghai Municipal Education Commission (Grant No. 2017-01-07-00-02-E00034). S. Pan acknowledges the support from the Academic Innovation Ability Enhancement Program for Excellent Doctoral Students of East China Normal University in 2021 (Grant No. 40600-30302-515100/141).

References

[1] C. I. Blaga, F. Catoire, P. Colosimo et al., "Strong-field photoionization revisited," *Nature Physics*, vol. 5, no. 5, pp. 335–338, 2009.

[2] W. Quan, Z. Lin, M. Wu et al., "Classical aspects in above-threshold ionization with a midinfrared strong laser field," *Physical Review Letters*, vol. 103, no. 9, article 093001, 2009.

[3] F. H. M. Faisal, "Ionization surprise," *Nature Physics*, vol. 5, no. 5, pp. 319-320, 2009.

[4] C. P. Liu and K. Z. Hatsagortsyan, "Origin of unexpected low energy structure in photoelectron spectra induced by midinfrared strong laser fields," *Physical Review Letters*, vol. 105, no. 11, article 113003, 2010.

[5] T. Yan, S. V. Popruzhenko, M. J. J. Vrakking, and D. Bauer, "Low-energy structures in strong field ionization revealed by quantum orbits," *Physical Review Letters*, vol. 105, no. 25, article 253002, 2010.

[6] A. Kästner, U. Saalmann, and J. M. Rost, "Electron-energy bunching in laser-driven soft recollisions," *Physical Review Letters*, vol. 108, no. 3, article 033201, 2012.

[7] C. Y. Wu, Y. D. Yang, Y. Q. Liu et al., "Characteristic spectrum of very low-energy photoelectron from above-threshold ionization in the tunneling regime," *Physical Review Letters*, vol. 109, no. 4, article 043001, 2012.

[8] L. Guo, S. S. Han, X. Liu et al., "Scaling of the low-energy structure in above-threshold ionization in the tunneling regime: theory and experiment," *Physical Review Letters*, vol. 110, no. 1, article 013001, 2013.

[9] W. Becker, S. P. Goreslavski, D. B. Milošević, and G. G. Paulus, "Low-energy electron rescattering in laser-induced ionization," *Journal of Physics B: Atomic, Molecular and Optical Physics*, vol. 47, no. 20, article 204022, 2014.

[10] B. Schütte, C. Peltz, D. R. Austin et al., "Low-energy electron emission in the strong-field ionization of rare gas clusters," *Physical Review Letters*, vol. 121, no. 6, article 063202, 2018.

[11] A. Staudte, S. Patchkovskii, D. Pavičić et al., "Angular tunneling ionization probability of fixed-in-space H_2 molecules in intense laser pulses," *Physical Review Letters*, vol. 102, no. 3, article 033004, 2009.

[12] J. Wu, M. Magrakvelidze, L. P. H. Schmidt et al., "Understanding the role of phase in chemical bond breaking with coincidence angular streaking," *Nature Communications*, vol. 4, no. 1, 2013.

[13] Q. Ji, S. Pan, P. He et al., "Timing dissociative ionization of H_2 using a polarization-skewed femtosecond laser pulse," *Physical Review Letters*, vol. 123, no. 23, article 233202, 2019.

[14] Y. Mi, P. Peng, N. Camus et al., "Clocking enhanced ionization of hydrogen molecules with rotational wave packets," *Physical Review Letters*, vol. 125, no. 17, article 173201, 2020.

[15] S. Pan, W. Zhang, H. Li et al., "Clocking dissociative above-threshold double ionization of H_2 in a multicycle laser pulse," *Physical Review Letters*, vol. 126, no. 6, article 063201, 2021.

[16] B. Feuerstein, T. Ergler, A. Rudenko et al., "Complete characterization of molecular dynamics in ultrashort laser fields," *Physical Review Letters*, vol. 99, no. 15, article 153002, 2007.

[17] J. McKenna, F. Anis, B. Gaire et al., "Suppressed dissociation of H_2^+ vibrational states by reduced dipole coupling," *Physical Review Letters*, vol. 103, no. 10, article 103006, 2009.

[18] A. Giusti-Suzor, X. He, O. Atabek, and F. H. Mies, "Above-threshold dissociation of H_2^+ in intense laser fields," *Physical Review Letters*, vol. 64, no. 5, pp. 515–518, 1990.

[19] A. Zavriyev, P. H. Bucksbaum, H. G. Muller, and D. W. Schumacher, "Ionization and dissociation of H_2 in intense laser fields at 1.064 μm, 532 nm, and 355 nm," *Physical Review A*, vol. 42, no. 9, pp. 5500–5513, 1990.

[20] P. Lu, J. Wang, H. Li et al., "High-order above-threshold dissociation of molecules," *Proceedings of the National Academy of Sciences of the United States of America*, vol. 115, no. 9, pp. 2049–2053, 2018.

[21] P. H. Bucksbaum, A. Zavriyev, H. G. Muller, and D. W. Schumacher, "Softening of the H_2^+ molecular bond in intense laser fields," *Physical Review Letters*, vol. 64, no. 16, pp. 1883–1886, 1990.

[22] K. Sändig, H. Figger, and T. W. Hänsch, "Dissociation dynamics of H_2^+ in intense laser fields: investigation of photofragments from single vibrational levels," *Physical Review Letters*, vol. 85, no. 23, pp. 4876–4879, 2000.

[23] R. Dörner, V. Mergel, O. Jagutzki et al., "Cold target recoil ion momentum spectroscopy: a 'momentum microscope' to view atomic collision dynamics," *Physics Reports*, vol. 330, no. 2-3, pp. 95–192, 2000.

[24] J. Ullrich, R. Moshammer, A. Dorn, R. Dörner, L. P. H. Schmidt, and H. Schmidt-Böcking, "Recoil-ion and electron momentum spectroscopy: reaction-microscopes," *Reports on Progress in Physics*, vol. 66, no. 9, pp. 1463–1545, 2003.

[25] G. Karras, M. Ndong, E. Hertz et al., "Polarization shaping for unidirectional rotational motion of molecules," *Physical Review Letters*, vol. 114, no. 10, article 103001, 2015.

[26] M. V. Ammosov, N. B. Delone, and V. P. Krainov, "Tunnel ionization of complex atoms and atomic ions in an electromagnetic field," *Soviet Physics, Journal of Experimental and Theoretical Physics*, vol. 64, pp. 1191–1196, 1986.

[27] I. A. Bocharova, A. S. Alnaser, U. Thumm et al., "Time-resolved Coulomb-explosion imaging of nuclear wave-packet dynamics induced in diatomic molecules by intense few-cycle laser pulses," *Physical Review A*, vol. 83, no. 1, article 013417, 2011.

[28] A. M. Sayler, P. Q. Wang, K. D. Carnes, B. D. Esry, and I. Ben-Itzhak, "Determining laser-induced dissociation pathways of multielectron diatomic molecules: application to the dissociation of O_2^+ by high-intensity ultrashort pulses," *Physical Review A*, vol. 75, no. 6, article 063420, 2007.

[29] X. Gong, P. He, Q. Song et al., "Two-dimensional directional proton emission in dissociative ionization of H_2," *Physical Review Letters*, vol. 113, no. 20, article 203001, 2014.

[30] C. Hu, W. Li, W. Zhang, X. C. Gong, J. Wu, and F. He, "Angle-resolved Rabi flopping in strong-field dissociation of molecules," *Physical Review A*, vol. 103, no. 4, article 043122, 2021.

[31] R. Kosloff and H. Tal-Ezer, "A direct relaxation method for calculating eigenfunctions and eigenvalues of the Schrödinger equation on a grid," *Chemical Physics Letters*, vol. 127, no. 3, pp. 223–230, 1986.

[32] W. H. Press, S. A. Teukolsky, W. T. Vetterling, and B. P. Flannery, *Numerical Recipes: The Art of Scientific Computing*, Cambridge University Press, Cambridge, 3rd edition, 2007.

[33] H. Xu, E. Lötstedt, A. Iwasaki, and K. Yamanouchi, "Sub-10-fs population inversion in N_2^+ in air lasing through multiple state coupling," *Nature Communications*, vol. 6, 2015.

[34] T. Xu and F. He, "Dissociation of D_2^+ by UV and THz light pulses," *Physical Review A*, vol. 88, article 043426, 2013.

[35] C. F. de Morisson Faria and I. Rotter, "High-order harmonic generation in a driven two-level atom: periodic level crossings and three-step processes," *Physical Review A*, vol. 66, no. 1, article 013402, 2002.

[36] A. S. Alnaser, X. M. Tong, T. Osipov et al., "Laser-peak-intensity calibration using recoil-ion momentum imaging," *Physical Review A*, vol. 70, no. 2, article 023413, 2004.